Science Advances

AAAS

Supplementary Materials for

Crystal structure of the human oxytocin receptor

Yann Waltenspühl, Jendrik Schöppe, Janosch Ehrenmann, Lutz Kummer, Andreas Plückthun*

*Corresponding author. Email: plueckthun@bioc.uzh.ch

This PDF file includes:
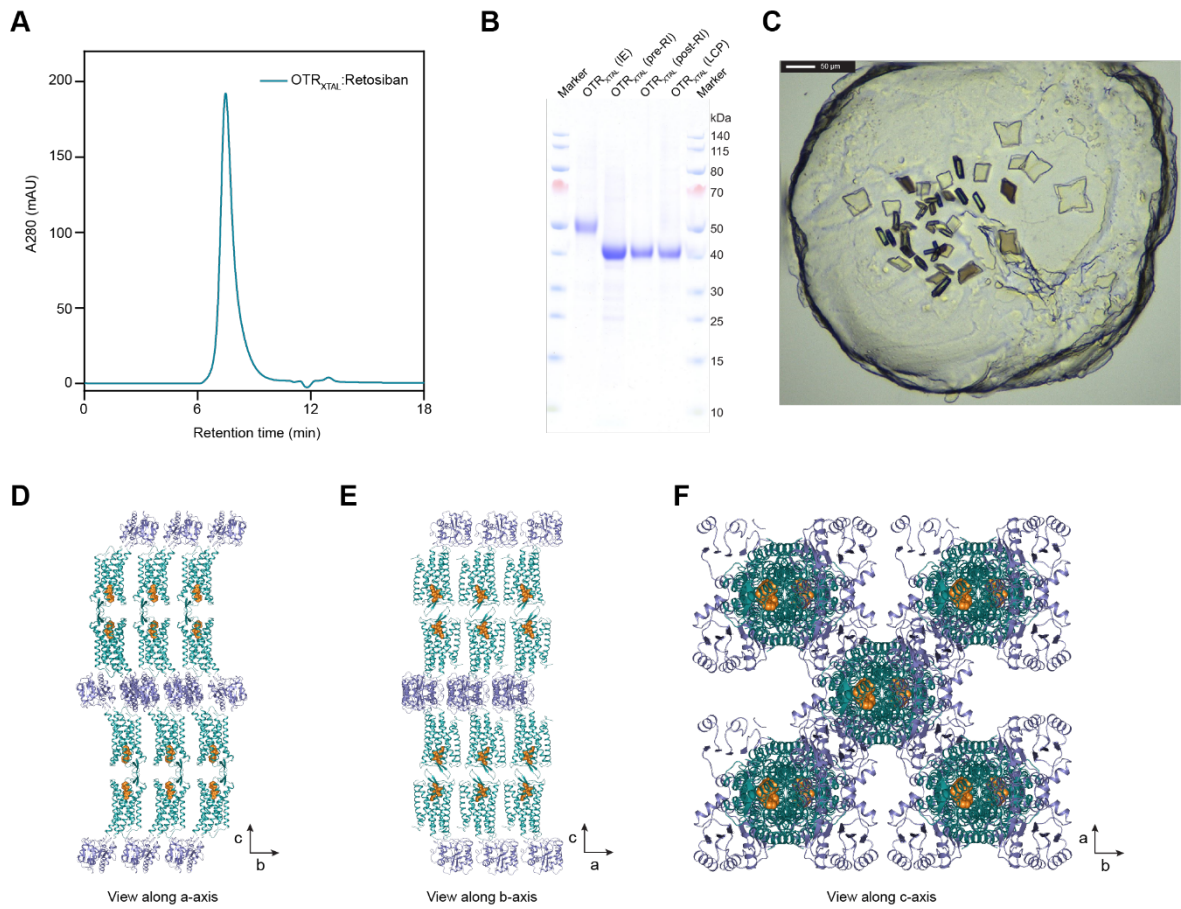
Figs. S1 to S6
Tables S1 to S5

Fig. S1 | OTR crystallisation

(**A**) Size exclusion profile of purified OTR:retosiban complex. (**B**) SDS-PAGE gel of purified OTR:retosiban complex. Loading scheme from left to right: IMAC eluate (IE), IMAC eluate after treatment with 3C protease and PNGaseF (pre-RI), reverse IMAC eluate (RI), concentrated reverse IMAC eluate used for crystallisation (LCP). **c**, Bright-field image of OTR:retosiban crystals in lipidic cubic phase. (**C**) Packing of OTR:retosiban crystals as viewed along the a axis of the unit cell. (**D**) Packing of OTR:retosiban crystals as viewed along the b axis of the unit cell. (**E**) Packing of OTR:retosiban crystals as viewed along the c axis of the unit cell.
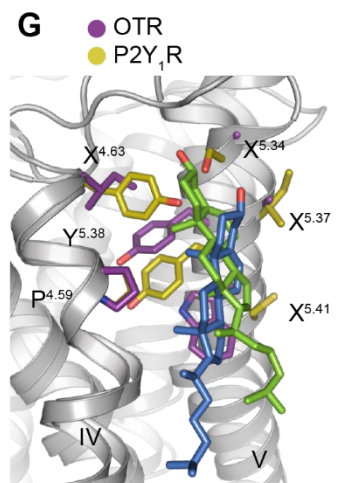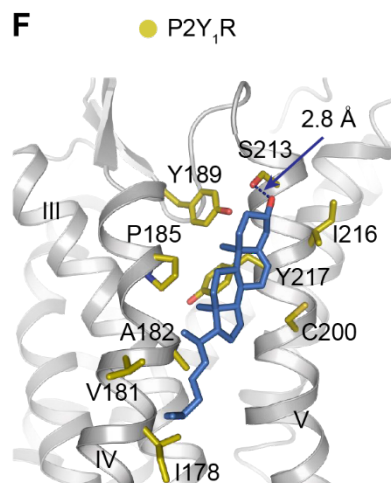
A

retosiban

B

I201 V
F175 IV
I204
Q171
K116 III
Q295
F291 M123 Q119
W288 Q92
VII II

C

cholesterol

D

I192
V190
F191 W195
I174 Y200 A199 V
P170
W203 IV III

E ● OTR

3.2 Å
I192
V190 W195
F191
III
I174
P170 Y200 A199
W203
IV V

F ● P2Y₁R

2.8 Å
Y189
III S213
I216
P185 Y217
A182 C200
V181
IV I178 V

G ● OTR ● P2Y₁R

X⁴·⁶³ X⁵·³⁴
Y⁵·³⁸
X⁵·³⁷
P⁴·⁵⁹
X⁵·⁴¹
IV V
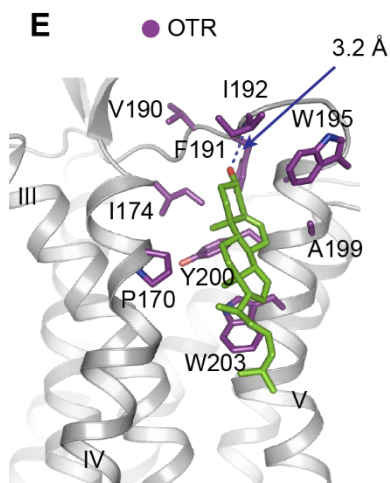
Fig. S2 | Electron density maps of the extracellular ligand binding pocket the cholesterol binding site of OTR and comparison of cholesterol binding sites of OTR and P2Y$_1$R
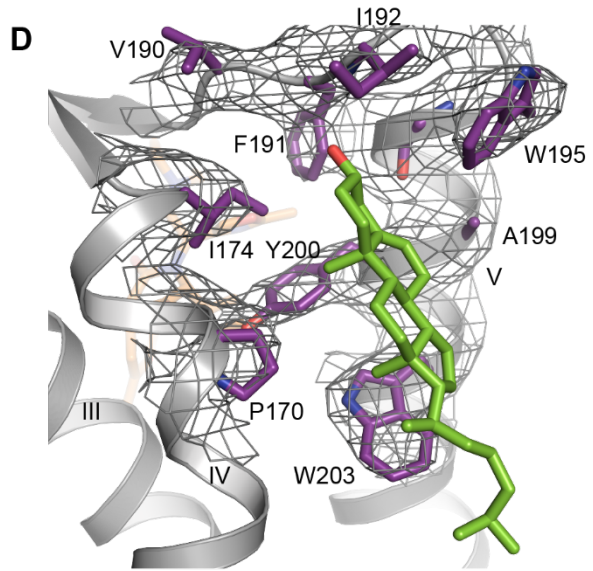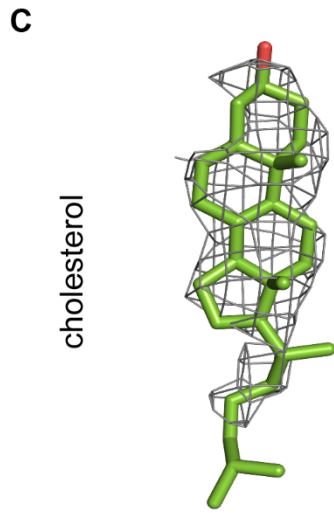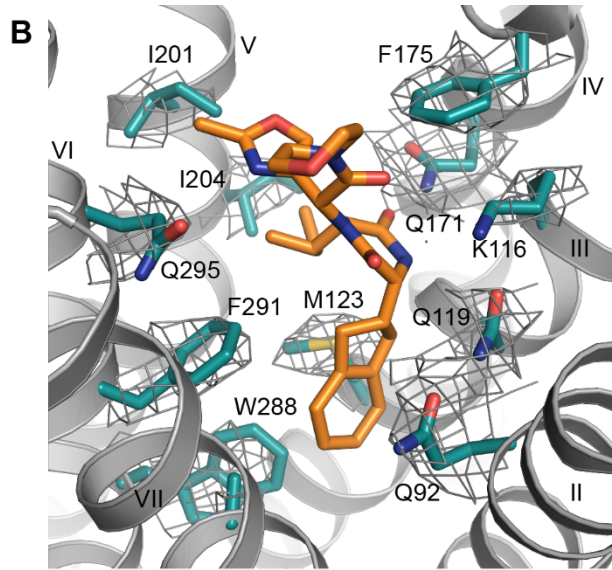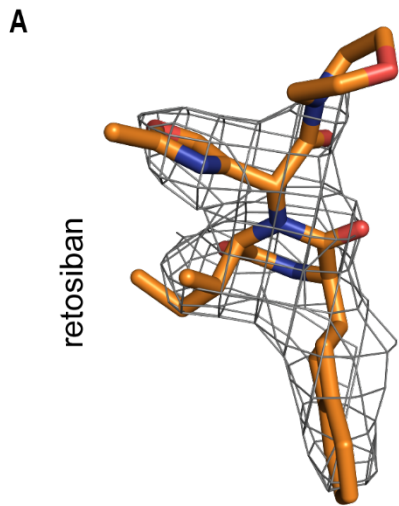
(**A**) Retosiban with 2Fo-Fc electron density map contoured at 1.0 σ. (**B**) 2Fo-Fc electron density map contoured at 1.0 σ for OTR residues interacting with retosiban. Oxygen and nitrogen atoms are coloured in red and blue, respectively. (**C**) Cholesterol with 2Fo-Fc electron density map contoured at 1.0 σ. (**D**) 2Fo-Fc electron density map contoured at 1.0 σ for OTR residues interacting with cholesterol. (**E & F**) Cholesterol binding site of (E) OTR and (F) P2Y$_1$R (PDB ID: 4XNV) in between transmembrane helices IV and V. Hydrogen bonds are indicated by dashed blue lines. (**G**) Overlay of cholesterol bindings sites of OTR (violet) and P2Y$_1$R (yellow). Cholesterol molecules are coloured in green (OTR) or in blue (P2Y$_1$R), respectively.

A OX$_2$R:Suvorexant   180°

B Y$_1$R:BMS-193885   180°

C NK$_1$R:Aprepitant   180°

D NTS$_1$R:NTS8-13   180°

E β$_1$-AR:cyanopindolol   180°

F μ-OR:BFT   180°

G Suvorexant

BMS-193885

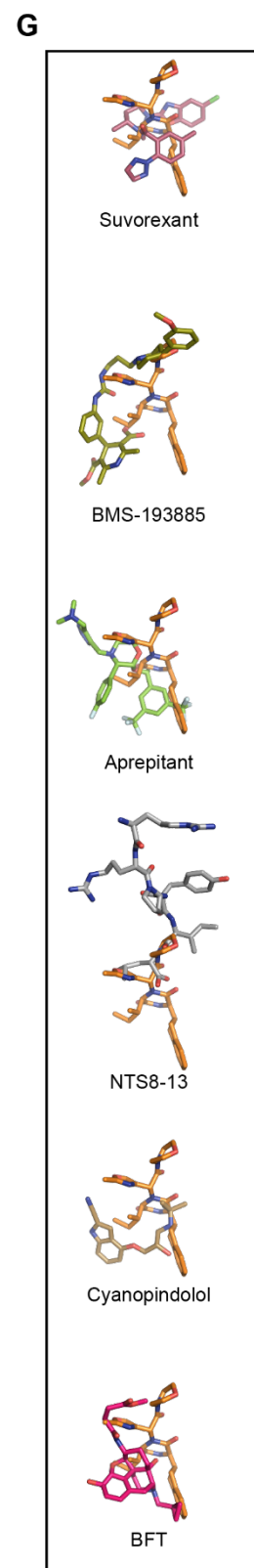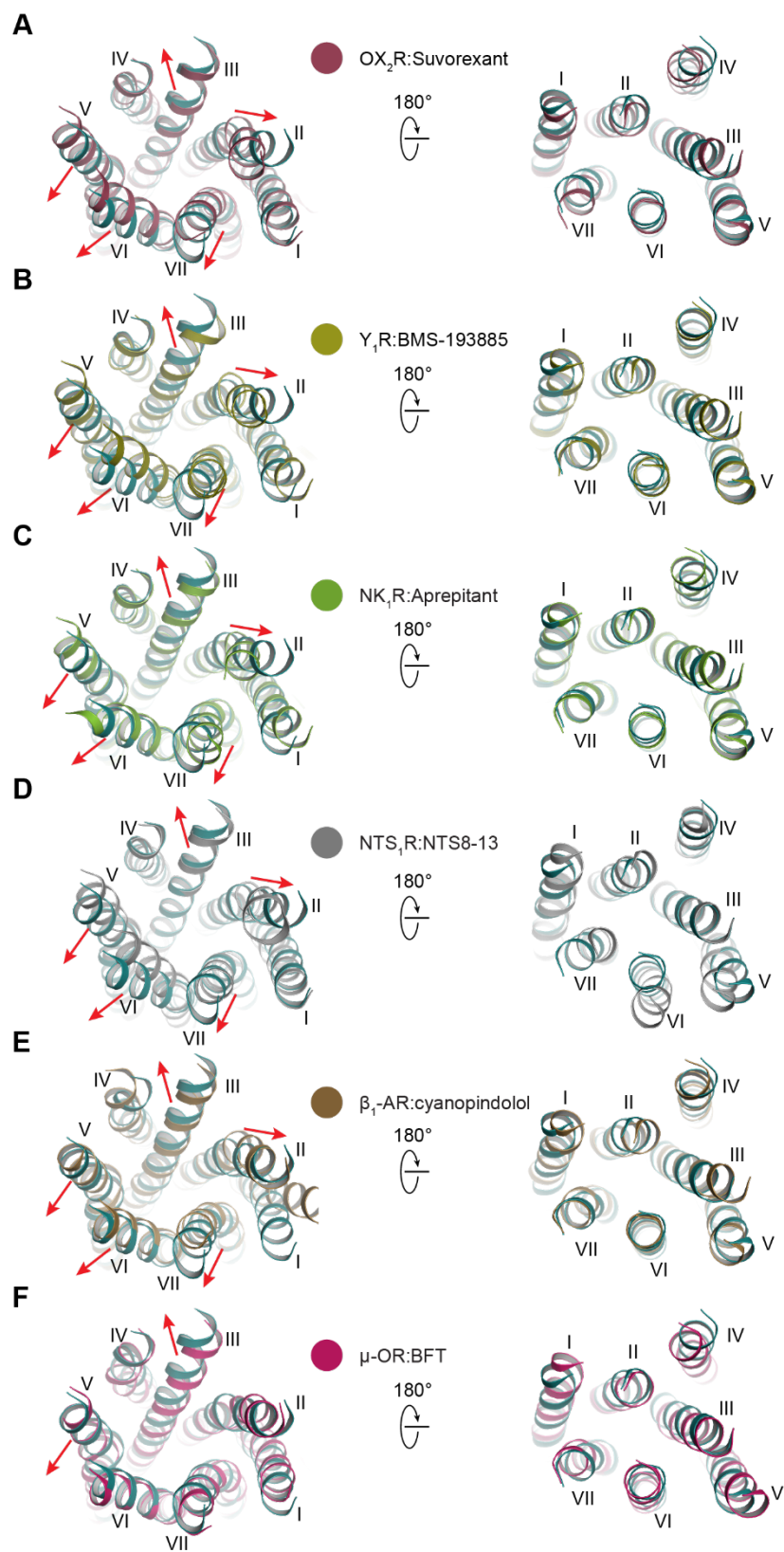Aprepitant

NTS8-13

Cyanopindolol

BFT

Fig. S3 | Comparison of transmembrane helix conformations shaping the extracellular binding site of OTR to other peptidergic and aminergic GPCRs

As viewed from the extracellular space (left) and from the cytoplasm (right). Red arrows indicate shift of OTR extracellular helix tips relative to reference receptor.

(**A-F**) Structural superposition of OTR:retosiban (coloured in cyan) with previously reported class A GPCR crystal structures yields root-mean-square deviations (RMSD, summarised in Table S1) for backbone atoms of (A) 2.7 Å to orexin 2 receptor, (B) 2.9 Å to neuropeptide Y Y1 receptor, (C) 1.6 Å to neurokinin 1 receptor, (D) 2.3 Å to neurotensin 1 receptor, (E) 2.6 Å to β_1-adrenergic receptor and (F) 2.6 Å to the μ-opioid receptor.

(**G**) Isolated ligands from the overlays in (A-F), as viewed from helix VI-VII (retosiban coloured in orange).
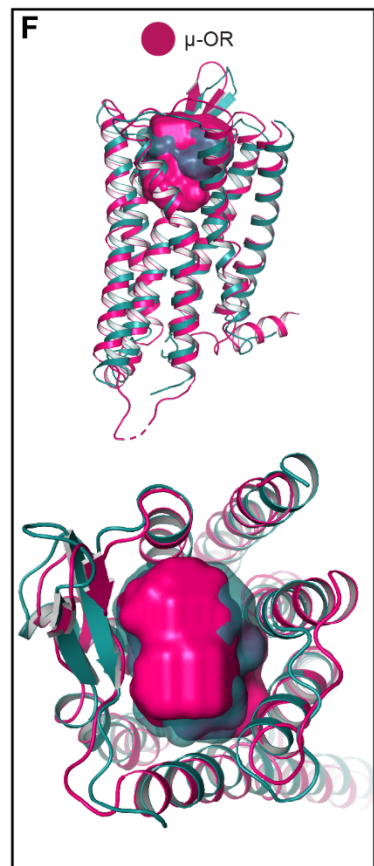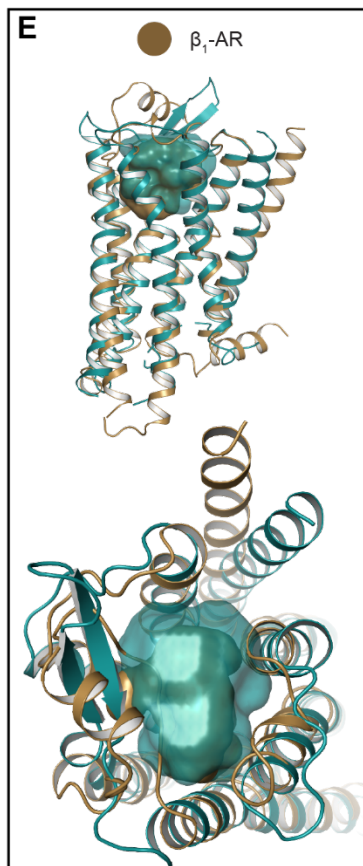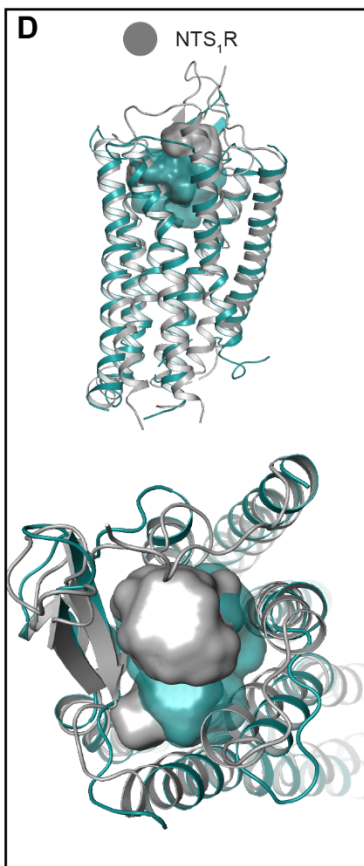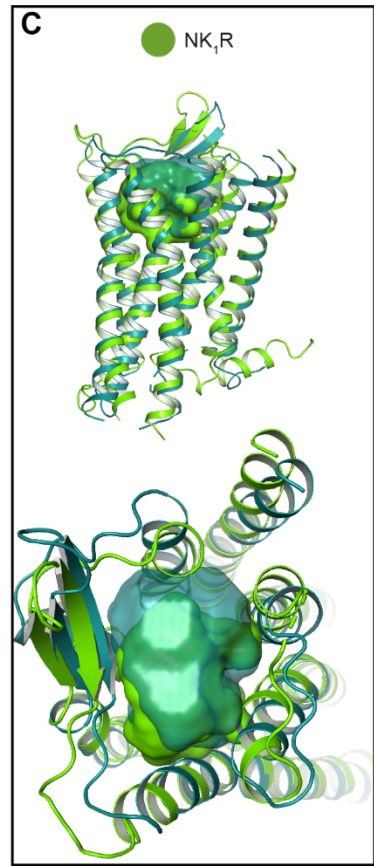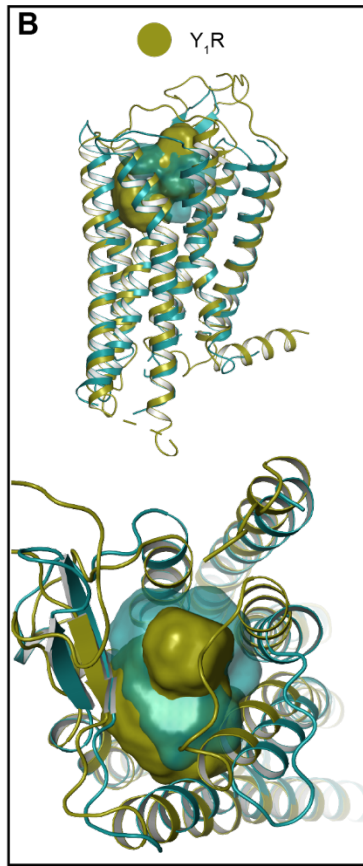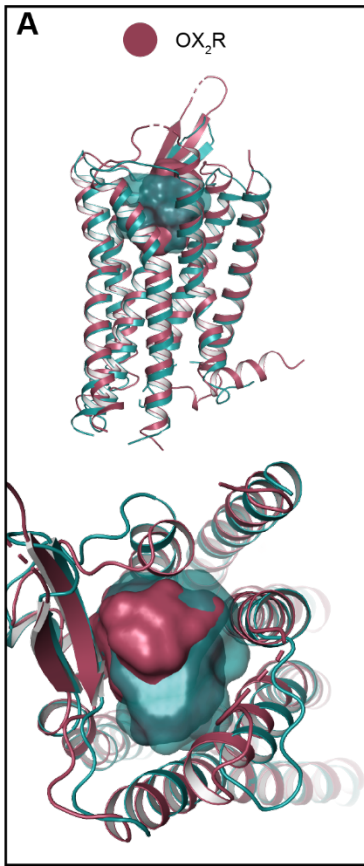
Fig. S4 | Volume differences of the extracellular binding pocket between OTR and other peptidergic and aminergic GPCRs

(**A-F**) In each panel an overlay of OTR:retosiban (coloured in cyan) with another GPCR is shown in cartoon representation, as viewed from the membrane plane (top) and from the extracellular space (bottom). The volumes of the extracellular ligand binding pockets are outlined as solid surfaces and highlighted in the respective colour of the receptors. Volumes were calculated using the program POVME 2.0 (Durrant, J.D. *et al*. *J. Chem. Theory Comput.* **10**, 5047-5056 (2014)). The structures overlayed with OTR:retosiban are (A) OX_2R:Suvorexant (PDB ID: 4S0V), (B) Y_1R:BMS-193885 (PDB ID: 5ZBH), **(**C) NK_1R:Aprepitant (PDB ID: 6HLO), (D) NTS_1R:NTS8-13 (PDB ID: 4GRV), (E) β_1 AR:cyanopindolol (PDB ID: 4BVN) and (F) μ-OR:BFT (PDB ID: 4DKL).

A

Species	Accession	1.34	1.35	1.36	B-W.	2.64	2.65	2.66		5.37	5.38	5.39	5.40	5.41	5.42	
Human (homo sapiens sapiens)	P30559	V	E	V		W	D	I		A	Y	I	T	W	I	OTR
Gorilla (Gorilla gorilla gorilla)	G3S6I2	V	E	V		W	D	I		A	Y	I	T	W	I	
Bovine (Bos taurus)	P56449	V	E	V		W	D	I		A	Y	I	T	W	I	
Mouse (mus musculus)	P97926	V	E	V		W	D	I		A	Y	V	T	W	I	
Human (homo sapiens sapiens)	P37288	L	E	I		W	D	I		A	Y	V	T	W	M	V₁ₐR
Gorilla (Gorilla gorilla gorilla)	XP_018893576.1#	L	E	I		W	D	I		A	Y	V	T	W	M	
Bovine (Bos taurus)	A2VDS9	L	E	I		W	D	I		A	Y	V	T	W	M	
Mouse (mus musculus)	Q62463	L	E	V		W	D	I		A	Y	V	T	W	M	
Turkey (Meleagris gallopavo)	G3USG7	V	E	V		W	D	I		A	Y	V	T	W	I	Homologues
Zebrafish (Danio rerio)	E4W699	V	E	V		W	D	I		A	Y	I	T	W	I	
King cobra (Ophiophagus hannah)	V8P3C6	V	E	V		W	D	I		A	Y	V	T	W	M	
Coelacanth (Latimeria chalumnae)	XP_005988002.1#	V	E	V		W	D	I		A	Y	V	T	W	I	
Xenopus (Xenopus laevis)	XP_018116839.1#	V	E	V		W	D	I		T	Y	I	T	W	I	
Snail (Lymnaea stagnalis)	AAA91998.1#	I	E	I		S	D	V		A	Y	I	T	W	V	
Ant (Harpegnathos saltator)	XP_011151734.1#	W	E	I		W	D	I		A	Y	I	T	W	Y	
Beetle (Tribolium castaneum)	NP_001078830.1#	V	E	V		W	D	I		A	Y	V	T	W	Y	

Mam · Non-mammal vertebrates · Invertebrates

B

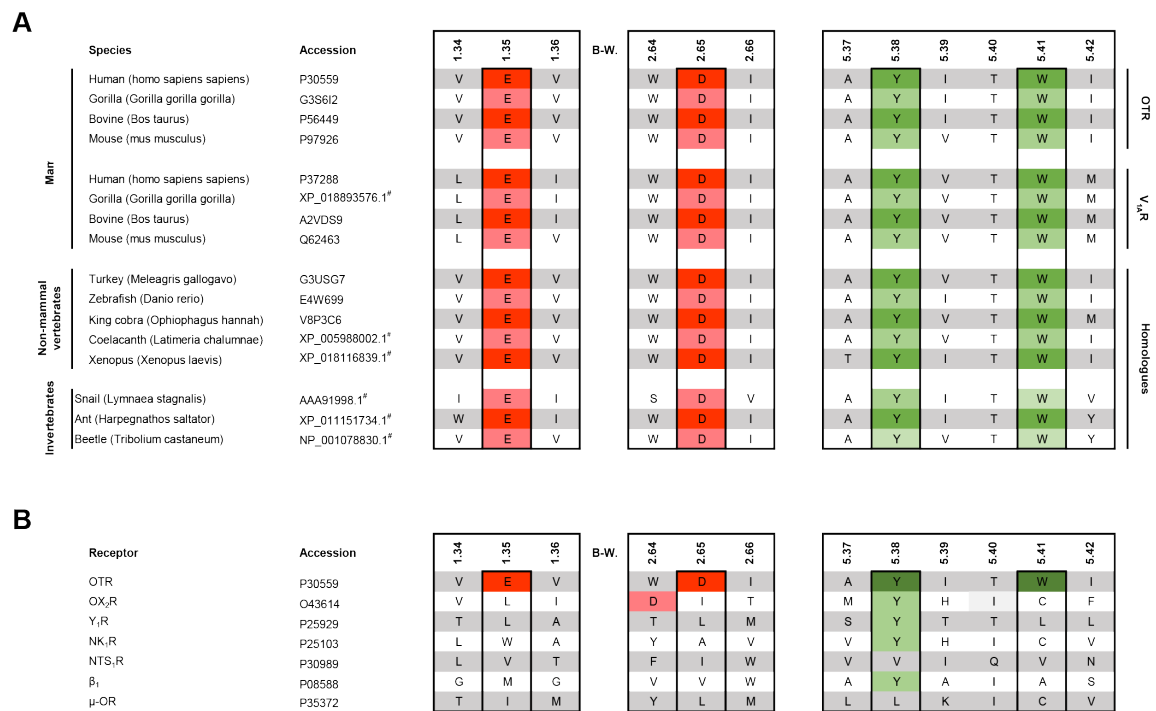| Receptor	Accession	1.34	1.35	1.36	B-W.	2.64	2.65	2.66		5.37	5.38	5.39	5.40	5.41	5.42
OTR	P30559	V	E	V		W	D	I		A	Y	I	T	W	I
OX₂R	O43614	V	L	I		D	I	T		M	Y	H	I	C	F
Y₁R	P25929	T	L	A		T	L	M		S	Y	T	T	L	L
NK₁R	P25103	L	W	A		Y	A	V		V	Y	H	I	C	V
NTS₁R	P30989	L	V	T		F	I	W		V	V	I	Q	V	N
β₁	P08588	G	M	G		V	V	W		A	Y	A	I	A	S
μ-OR	P35372	T	I	M		Y	L	M		L	L	K	I	C	V

Fig. S5 | Alignment of the divalent cation binding site of OTR

(**A**) Amino acid alignment of residues compromising the human OTR divalent cation coordination (red) and cholesterol binding (green) sites and several vertebrate and invertebrate homologues. Species name and UniProt Knowledgebase accession codes (www.uniprot.org) or NCBI reference sequence (marked with #, www.ncbi.nlm.nih.gov) are indicated in the first and second column, respectively. Amino acid residue alignment of positions according to the Ballesteros-Weinstein numbering scheme (BW) are indicated above the sequences. Residues of the OTR magnesium binding site are highlighted by black boxes. Acidic residues are highlighted in red. (**B**) Alignment with other peptidergic and aminergic GPCRs. Receptor name and UniProt Knowledgebase (www.uniprot.org) accession codes are indicated in the first and second column, respectively. Amino acid residue alignment of positions 1.34-1.36 and 2.64-2.66 according to the Ballesteros-Weinstein numbering scheme (BW) are indicated above the

sequences. Residues of the OTR magnesium binding site are highlighted by black boxes. Acidic
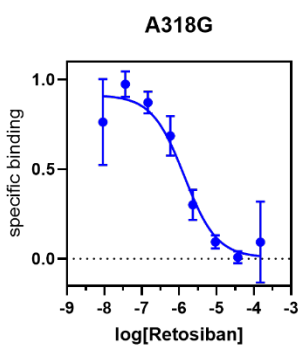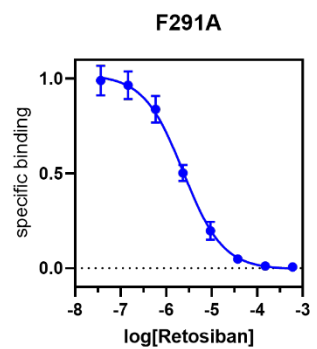
residues are highlighted in red.
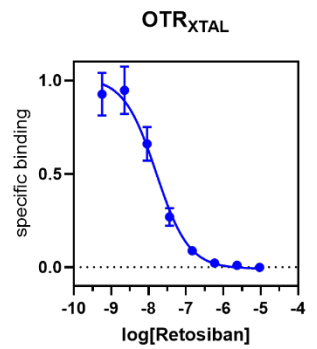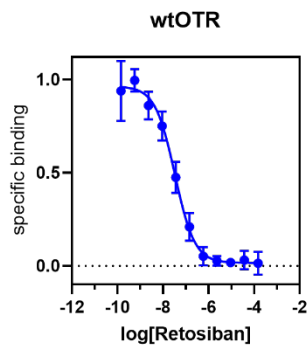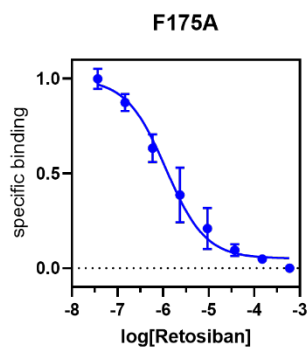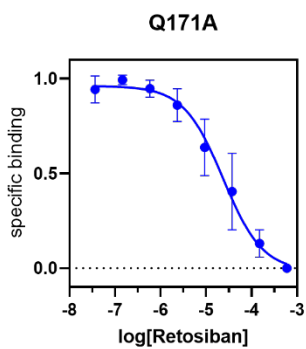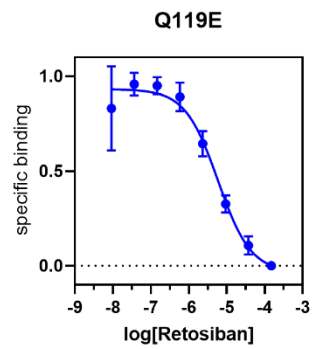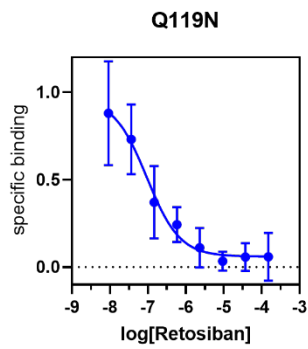
Fig. S6 | Binding of retosiban to wild-type and mutated OTR variants

Whole-cell competition binding experiments of different concentrations of unlabelled retosiban to HEK293T cells expressing wild-type (wtOTR) and mutated wtOTR variants, in the presence of fluorescently labelled PVA as a competitor. Binding curves are shown with 95% confidence intervals (CI) from 3 independent experiments performed as quadruplicates

Table S1 | Extracellular ligand binding pocket comparison.

receptor	RMSD [Å]	ligand	M_w [g mol^{-1}]	pocket volume [Å^3]	pocket volume relative to OTR [%]	PDB ID
OTR		retosiban	494.6	792	100	xx
OX2R	2.7	Suvorexant	450.9	569	72	4S0V
Y$_1$R	2.9	BMS-193885	590.7	605	76	5ZBH
NK$_1$R	1.6	Aprepitant	534.4	597	75	6HLO
NTS$_1$R	2.3	NTS8-13	817.0	433	55	4GRV
β$_1$-AR	2.6	Cyanopindolol	287.4	320	40	4BVN
μ-OR	2.6	BFT	468.5	911	115	4DKL

Root-mean-square deviations for backbone atoms (RMSD). Pocket volumes were calculated using the program POVME 2.0 (Durrant, J.D. *et al*. *J. Chem. Theory Comput.* **10**, 5047-5056 (2014)).

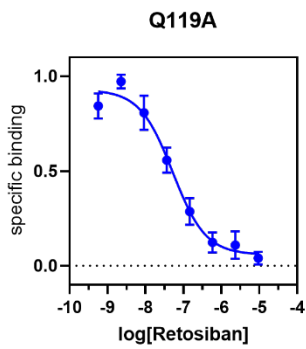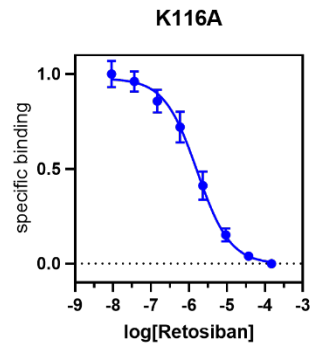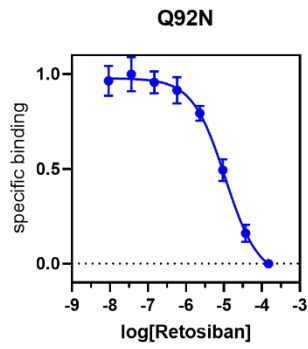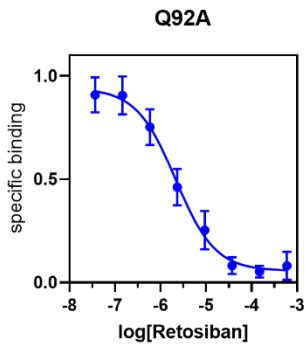**Table S2 | Binding of retosiban to wild-type and mutated OTR variants.**

construct	K_i retosiban [nM]	95% CI [nM]	K_D PVA-HL647 [nM]	B_{max} [%wtOTR]
Q92A	16.3	11.7 - 22.7	0.20 ± 0.12	6.9 ± 2.7
Q92N	517.6	411.1 - 650.8	0.32 ± 0.21	25.6 ± 0.4
K116A	195.4	158.4 - 241.3	0.84 ± 0.43	38.7 ± 0.1
Q119A	2.2	1.7 - 3.0	4.0 ± 1.1	9.1 ± 2.5
Q119N	31.1	11.1 - 85.4	2.8 ± 1.5	11 ± 0.2
Q119E	1142.9	767.3 - 1713	1.4 ± 0.46	33.1 ± 0.7
M123A	n.b.		n.b.	n.b.
Q171A	8260.4	5221 - 13060	88.5 ± 19.8	211.3 ± 59
F175A	11.7	8.9 - 15.3	199 ± 8.2	101.5 ± 43.9
I201A	n.b.		n.b.	n.b.
I204A	n.b.		n.b.	n.b.
F291A	1078.9	897.1 - 1299	21.9 ± 5.7	78.7 ± 19.5
A318G	40.5	25.2 - 65.3	0.38 ± 0.16	11.4 ± 0.3
wtOTR	2.6	2.0 - 3.3	0.58 ± 0.25	100 ± 26.3
OTR$_{XTAL}$	7.6	5.9 - 9.9	6.4 ± 3.3	387 ± 48.9

Whole-cell competition binding experiments of different concentrations of unlabelled retosiban to HEK293T cells expressing wild-type (wtOTR) and mutated wtOTR variants, in the presence of fluorescently labelled PVA as a competitor. Retosiban affinities are shown as mean values (K_i) with the respective 95% confidence intervals (CI) from 3 independent experiments performed in quadruplicates. *n.b.*, no binding. K_i values were calculated using the Cheng-Prusoff equation (Cheng, Y. & Prusoff, W.H. *Biochem. Pharmacol.* **22**, 3099-108 (1973)). PVA-HL647 saturation binding results to individual receptor variants are reported as K_D and $B_{max} \pm$ standard deviation from at least 3 independent experiments, each performed in triplicates.

Table S3 | Binding of agonist or antagonist to wild-type OTR and variants with mutations in the cholesterol binding site.

construct	surface expression [% of wtOTR]	B_{max} agonist [% of wtOTR]	B_{max} antagonist [% of wtOTR]
Y200A	111.3 ± 17.1	4.6 ± 4.1	0.7 ± 0.03
Y200H	108.0 ± 13.3	11.7 ± 1.5	3 ± 0.4
W203A	104.5 ± 16.5	19.2 ± 3.5	8.1 ± 0.5
W203H	101.3 ± 27.5	5.1 ± 1.5	0.2 ± 0.02
wtOTR	100 ± 13.9	100 ± 20.5	100 ± 3.5
OTR$_{XTAL}$	182.7 ± 38.5	471.4 ± 50.4	419.7 ± 44.2

Whole-cell specific binding experiments of agonist (HL488-Orn[8]-OT) and antagonist (HL647-PVA) on HEK293T cells expressing wild-type (wtOTR) and mutated wtOTR variants expressed as B_{max} values. In comparison the surface expression is also shown. Data are shown as mean values (surface expression and B_{max}) ± standard deviations (SD) from 3 independent experiments performed in triplicates.

Table S4 | Thermostability of OTR$_{XTAL}$ and variants with mutations in the cholesterol binding site.

construct	T$_m$ + CHS [°C]	T$_m$ - CHS [°C]
OTR$_{XTAL}$ Y200A	55.2 ± 0.8	44.5 ± 3.9
OTR$_{XTAL}$ W203A	61.2 ± 0.2	41.9 ± 3.1
OTR$_{XTAL}$	64.2 ± 0.6	43.7 ±1.9

CPM thermostability assay of OTR$_{XTAL}$ and mutated variants thereof in the presence or absence of the cholesterol analogue cholesteryl hemisuccinate (CHS). Data are shown as mean values (T$_m$) ± standard deviations (SD) from 3 independent experiments.

Table S5 | Ligand binding to wild-type OTR and variants with mutations in the Mg^{2+} binding site.

construct	Mg^{2+}	K_D [nM]	95% CI [nM]
wtOTR	+	1.2	0.9 - 1.5
wtOTR	–	27.9	22.7 - 34.4
E42A	+	19.1	15.0 - 24.4
E42A	–	29.6	23.0 - 38.4
D100A	+	26.2	23.8 - 28.8
D100A	–	30.8	28.1 - 33.7
E42D, D100E	+	16.4	11.2 - 24.1
E42D, D100E	–	28.4	20.1 - 40.7

Whole-cell specific binding experiment of agonist (HL488-Orn[8]-OT) to HEK293T cells expressing wild-type (wtOTR) and mutated wtOTR variants in the presence (+) or absence (-) of 3 mM Mg^{2+}. Data are shown as mean values (K_D) with the respective 95 % confidence interval (CI) from three independent experiments performed in triplicates.